HHS Public Access

Author manuscript

Allergy. Author manuscript; available in PMC 2023 April 25.

Published in final edited form as:

Allergy. 2018 February ; 73(2): 405–415. doi:10.1111/all.13310.

Mast cells and sphingosine-1-phosphate underlie prelesional remodeling in a mouse model of eczema

Piper A. Wedman[a], **Ahmed Aladhami**[a,b], **Alena P. Chumanevich**[a], **John W. Fuseler**[a], **Carole A. Oskeritzian**[a,*]

[a]Department of Pathology, Microbiology and Immunology, University of South Carolina School of Medicine, Columbia, South Carolina, USA

[b]University of Baghdad, Baghdad, Iraq

Abstract

Atopic dermatitis (AD) is a chronic skin inflammation that affects children and adults worldwide, but its pathogenesis remains ill-understood. We show that a single application of OVA to mouse skin initiates remodeling and cellular infiltration of the hypodermis measured by a newly developed computer-aided method. Importantly, we demonstrate that skin mast cell (MC) activation and local sphingosine-1-phosphate (S1P) are significantly augmented after OVA treatment in mice. Deficiency in sphingosine kinase (SphK)1, the S1P-producing enzyme, or in MC, remarkably mitigates all signs of OVA-mediated remodeling and MC activation. Furthermore, skin S1P levels remain unchanged in MC-deficient mice exposed to OVA. LPS-free OVA does not recapitulate any of the precursor signs of AD, supporting a triggering contribution of LPS in AD that, *per se*, suffice to activate local MC and elevate skin S1P. We describe MC and S1P as novel pathogenic effectors that initiate remodeling in AD prior to any skin lesions and reveal the significance of LPS in OVA used in most studies, thus mimicking natural antigen (Ag) exposure.

INTRODUCTION

Atopic dermatitis (AD) is a chronic inflammatory skin disease affecting 15–30% children and 2–10% adults world-wide (1–8). This complex disorder features hypersensitivity to environmental agents and immune dysfunction (1, 3, 5, 7, 9–11). Yet, the sequential events leading to eczematous lesions are not completely understood.

Interestingly, 70–80% of AD patients have increased levels of total serum IgE antibodies (1, 2, 5, 7, 12, 13). Perivascular accumulation of lymphocytes and mast cells (MC) are observed in chronic lesions (12). However, few studies have investigated the initial phase leading to lesions, including prior to IgE production (10, 14–18).

*Corresponding author: Carole A. Oskeritzian, Department of Pathology, Microbiology and Immunology, University of South Carolina School of Medicine, 6439 Garners Ferry Road, Columbia, South Carolina 29209, USA. Phone: (803) 216 3462. Fax: (803) 216 3428. Carole.Oskeritzian@uscmed.sc.edu.

AUTHORS CONTRIBUTIONS

PAW, AA and APC conducted experiments, acquired data and contributed to manuscript writing. PAW, AA and CAO analyzed data. JWF acquired and analyzed imaging data and contributed to manuscript writing. CAO designed research studies and wrote the manuscript.

The authors declare no competing financial interests.

With receptors for IgE (FcεRI) and other ligands, tissue-resident MC are critical first-line responders to inflammatory signals (19–22). Moreover, MC present the unique ability to produce and store vasoactive and cytoactive mediators in cytoplasmic granules prior to trauma and can neo-synthesize bioactive products upon activation (6, 11, 14, 20–24). We recently established MC and a potent sphingolipid metabolite, sphingosine-1-phosphate (S1P) at the nexus of inflammatory infiltration in early lung allergic responses (21). We previously reported that MC-derived S1P, produced by sphingosine kinase (SphK), can be exported out to amplify MC cytokine/chemokine production and regulate cell trafficking (21, 22, 25, 26). S1P can also activate MC independently of the canonical IgE/FcεRI pathway (13, 20, 21, 27).

In the current study, we investigated AD pathogenesis using a variation of a well-established human AD-like mouse model and collected skin samples for analysis after a *single* epicutaneous (EC) exposure to OVA Ag (16). We discovered a new pathogenic pathway leading to AD that links cell infiltration of the hypodermis to local MC activation and S1P elevation. Next, we examined skin remodeling in mice deficient for SphK1 or MC and after LPS-free OVA exposure and established an essential role for MC, S1P and LPS at the onset of AD.

RESULTS AND DISCUSSION

OVA triggers rapid skin remodeling and cellular infiltration

We previously reported that systemic Ag stimulation leads to early lung remodeling in sensitized mice (21). These studies prompted us to revisit the development of another inflammatory disease of atopic nature, AD, for which the initiating mechanisms remain ill-understood (28, 29). We found that epidermal and dermal thickening that is observed in the 49-day AD mouse model (15, 16), was already significant after one OVA application, compared to one saline treatment (Figures 1a–c).

We observed a marked cellular infiltration in the hypodermis, compared to saline controls (Figures 1a–c). We adapted our recently established image quantification method (30), to measure cellular infiltration (Figure 1d) in a defined region of interest (ROI) (circle in Figure 1e) sequentially moved across the entire hypodermis. Figure 1g shows whole hypodermis survey of infiltration in a representative saline-treated skin sample compared to an OVA-treated one, in which blood vessel (Bv)-containing ROI are depicted in red. Saline treatment triggered some infiltration, increased around Bv. The OVA application drastically increased hypodermal cell numbers, also around Bv (Figure 1g). The statistical validation of these results was demonstrated by analyzing multiple samples (Figures 1f, h).

Having previously established the relevance of fractal dimension to define morphometric descriptors (30), we reasoned fractals or measures of space filling capacity could also represent an accurate method to quantify cellular infiltration. Figures 1i–j describe the procedure established to isolate nuclei/cells. Next, binary images (Figure 1k) were generated to calculate fractal dimensions (D) of ROI by quantifying the structural density of the “objects” (nuclei) or cellular infiltration. Figure 1l independently confirmed the increased cellular infiltration substantiated in Figures 1f–h after OVA treatment as measured by D

values of multiple skin samples. The discriminatory performance of D was further validated in Figure 1m, also showing increased infiltration around the Bv.

Importantly, the present study analyzed prelesional skin specimens, therefore identifying novel histo-pathological mechanisms of AD. We described a new morphometric method to quantify rather than score cellular infiltration and uncovered a prevalent although previously unnoticed hypodermal infiltration after a single OVA treatment, suggesting an important function for the hypodermis at the onset of AD. We propose this initial infiltration, also reported in acutely inflamed airways (21), could constitute a novel target to prevent disease manifestation.

OVA stimulates local and systemic chemokines

We next investigated chemokine expression in skin samples. Skin mRNA expression for CCL2, CCL3 and CCL5, three members of the chemokine network we previously identified as major contributors to airway inflammation (21) were all significantly increased after OVA exposure (Figure 2a). Interestingly, skin CCL2 (Figure 2b) and CCL3 (Figure 2c) (but not CCL5 (data not shown)) protein levels were also increased upon OVA application, compared to saline controls. As expected, circulating chemokine levels did not exactly corroborate local levels. Serum CCL2 levels remained unchanged after EC OVA (Figure 2d), whereas serum CCL3 and CCL5 were enhanced (Figures 2e–f). Recently, a meta-analysis also described increased chemokine mRNA expression in patients with AD (31). CCL2 and CCL3 genes were also identified in patients with moderate-to-severe AD by next-generation RNA-sequencing (32). Combined with our finding, these studies also suggest an important role of infiltration to establish AD.

OVA exposure elicits significant IgE-independent skin MC degranulation and S1P elevation

We found that mRNA coding for the α chain of FcεRI (FcεRIα) was significantly up-regulated in OVA-treated mouse skin samples (Figure 3a). Importantly, the α chain is responsible for IgE binding to its receptor and initiates MC activation during allergic responses (33). Although expressed by Langerhans (34) and other cells (35), we reasoned that skin-resident MC could also contribute to the enhanced FcεRIα mRNA detection in these samples. Microscopy examination of methylene blue (MB)-stained skin sections revealed that metachromatic MC were distributed throughout the skin layers, irrelevant of treatment (Figures 3b–c). Using our previously reported MC morphometrics, skin sections were analyzed for MC activation (30). Figures 3b–c show representative examples of resting (green-framed insert, circle and arrow) MC and degranulated (red-framed insert, circle and arrow) MC. Figure 3d demonstrated that hypodermal MC were significantly more degranulated after OVA than after saline application or other controls (Supplemental Figure 1a). While it has been shown that AD features increased perivascular MC (36, 37), MC numbers were unaltered in either treatment (data not shown). Of note, a recent report delineated a protective role for MC during the development of spontaneous AD-like disease in a transgenic mouse model but did not measure local MC activation (38). Our finding of increased *in situ* MC degranulation at this early subclinical stage of AD was novel and intriguing. As expected, seven days of OVA exposure did not suffice to enhance circulating

IgE levels (Figure 3e), compared to its abundant detection after 3 OVA treatments (Figure 3e) as originally described (16).

MC can be activated by S1P, an influential sphingolipid metabolite resulting from the phosphorylation of its precursor sphingosine by SphK (20, 21, 25, 27, 39). Quantitative lipid analysis using lipidomics mass spectrometry (40), revealed that S1P was significantly increased in mouse skin after one exposure to OVA, compared to controls (Figure 3f and Supplemental Figure 1b). In agreement, SphK1 skin mRNA expression was also augmented after a single OVA application (Figure 3g) while others coding for S1P catabolizing pathways remained unchanged ((41, 42) Supplemental Figure 2). We have shown that S1P-mediated MC activation led to the release of pro-inflammatory cytokines, including IL-6 and TNF, as well as cell recruiting chemokines (20, 21, 25, 43). MC may also serve as a local source of S1P (25, 26), including when activated by mechanical stress such as tape-stripping, and induce leukocyte rolling (44). MC are established chemokine producers in chronic AD (14, 19) and mediate leukocyte recruitment (22, 45–48), although dispensable in a genetic mouse model (49). In the present study, it is noteworthy that local chemokine detection and MC activation occurred prior to IgE production. While augmented in most AD patients (5, 7, 12), our data suggest that IgE may contribute to AD progression rather than initiation. Importantly, our results strongly support MC and S1P as early contributors to the development of pre-AD-related skin alterations.

SphK1 or MC deficiency protects against OVA-driven skin remodeling and infiltration

To determine the relevance of S1P in these pre-symptomatic changes, we repeated the adapted AD protocol in SphK1 KO mice (50), of genetic background similar to the WT mice used so far (Figures 1–3). SphK1 deficiency mitigated OVA-initiated skin remodeling (Figures 4a *vs.* 1c). The SphK1-null hypodermis surveying revealed a slight but significant increase in nuclei (i.e., cell) numbers after OVA, compared to saline-treated skins (Figure 4b), that was less pronounced than in SphK1-sufficient mice (Figures 4b *vs.* 1f) and absent around the Bv (Figures 4c *vs.* 1h). Consistent with these results, the pattern of OVA-restricted chemokine gene induction in corresponding WT skin samples (Figure 2a) was not observed in SphK1 KO mouse skins (Figure 4d). Importantly, genetic ablation of SphK1 prevented OVA-initiated local up-regulation of FcεRIα mRNA expression (Figures 4d *vs.* 3a) and skin MC degranulation, also observed after administration of the selective SphK1 pharmacological inhibitor PF-543 ((51), Figures 4e *vs.* 3d). These results strongly suggest that S1P is a driving mediator of IgE-independent skin remodeling and infiltration through local skin MC degranulation in AD pathogenesis.

To investigate MC's contribution to skin remodeling, we conducted OVA or saline EC exposure of MC-deficient $Kit^{W\text{-}sh/W\text{-}sh}$ (52) mice. Although some epidermal thickening was observed, $Kit^{W\text{-}sh/W\text{-}sh}$ dermal layers were unaltered (Figure 4f), compared to MC-sufficient mice of similar genetic background (Figure 1c). Furthermore, MC deficiency prevented cellular infiltration of the hypodermis (Figures 4g–h), suggesting a critical role of MC in skin inflammation. This was further confirmed by the absence of OVA-induced up-regulation of chemokine, FcεRIα and SphK1 mRNA levels (Figure 4i). It is noteworthy that skin-associated S1P levels were significantly lower and not increased upon OVA application

in *Kit*$^{W\text{-}sh/W\text{-}sh}$ mice (Figure 4j), compared to the corresponding WT mice (Figure 3f), supporting skin MC as a relevant local source of S1P.

Thus, it is tempting to speculate that MC may act as causative agents of inflammatory response of the skin, similar to our recent report pertaining to lung allergic responses (21). Moreover, local elevations of S1P in inflamed skins, absent in SphK1-null or PF-543-treated mice (data not shown), may contribute to early MC activation at the inception of AD, prompting MC themselves to further produce S1P. Keratinocytes (53) and Langerhans cells (54) could also contribute to local S1P release. Nonetheless, our results suggest an important function for MC-derived S1P at the onset of AD, linking S1P and chemokines to early skin remodeling, setting the stage for disease progression. Decreased S1P in human AD has been evoked but not measured (55). In agreement with previous studies (25, 56), our data evoke a strong interdependency not only between 1) the presence of SphK1 and skin MC activation but also 2) skin S1P level alterations and the presence of MC. We propose local S1P and MC are likely triggering components of skin remodeling in early AD.

Cellular infiltration, MC activation and local S1P elevation are abrogated in mice treated with lipopolysaccharide (LPS)-free OVA

Yoon *et al.* recently established that endogenous toll-like receptor (TLR)4 ligands are essential to epidermal thickening observed in EC-sensitized skin after tape-striping (57). Furthermore, commercial-grade OVA, used in this and most studies, contains high LPS levels, a TLR4 ligand (58). To investigate the LPS contribution to the early skin inflammation upon EC OVA exposure, experiments were repeated using LPS-free OVA. EC LPS-free OVA-triggered hypodermal infiltration was similar to the one observed in saline-treated animals (Figures 5a–b). Moreover, local MC were not activated (Figure 5c) and S1P and SphK1 and S1P lyase Sgpl1 mRNA levels remained unaltered following LPS-Free OVA exposure (Figures 5d–e). S1P phosphatase Sgpp1 (but not Sgpp2) mRNA levels were significantly augmented in LPS-free OVA-treated samples (Figure 5e), perhaps explaining the lack of S1P increase (Figure 5d). EC LPS application recapitulated enhanced skin MC degranulation and S1P measured after EC OVA administration (Supplemental Figures 3a and 3b, respectively). These results suggest that ~~the~~ LPS co-administered with OVA Ag participated in early skin inflammatory responses. As most environmental Ag penetrate the body likely combined with LPS, this mimics natural Ag exposure. Several studies have investigated the effect of LPS “contamination” of OVA in allergic responses. While some studies reported that LPS/TLR4 signaling prime pro-inflammatory responses to OVA (59, 60), others described protective effects of LPS (58). *Staphylococcus* strains residing on healthy skins produce a peptide inhibiting AD-patient skin-colonizing *Staphylococcus aureus* growth (61). Skin microbiome may promote local MC maturation (62). Our study is the first to compare the effects of OVA to LPS-free OVA in a mouse model of skin inflammation. Furthermore, our results suggest that LPS exposure may prime initial inflammatory responses, as recently suggested (57), and promote local MC activation and endogenous S1P production. Topical exogenous S1P administration attenuated contact dermatitis in a hapten-induced murine AD-like model (63). We propose that endogenously produced S1P can exert varied pro-inflammatory functions, compared to exogenously applied, anti-inflammatory S1P.

Topical application of Fingolimod (FTY720), a structural analog of sphingosine also phosphorylated by SphK, acts as an S1P receptor (R) agonist and attenuates skin inflammation (64). FTY720 treatment prevented enhanced MC degranulation after OVA treatment (Supplemental figure 4a). FTY720 can be phosphorylated *in vivo* to activate S1PR2 and repress inflammation (65, 66). FTY720 did not alter skin S1P perhaps because of its inhibitory effect on Sgpl1 that results in S1P increase ((67) Supplemental figure 4b).

Small but statistically significant structural and molecular alterations between saline and OVA treatment are expected, as these pathogenic events occur prior to any overt sign of disease. We also observed a range of responses among mice for many of the parameters measured. However, careful analysis of the data did not indicate any potential classification into high and low responders. These primary and newly uncovered responses could not be compared to the large differences reported when comparing acute to chronic AD skin lesions and further emphasize the relevance of our findings to pre-symptomatic AD pathogenesis. These initial signs of skin remodeling set the stage to forthcoming clinical features of AD, including eczematous lesions observed in this preclinical model after 3 OVA exposures and in human AD. These findings highlight perhaps new prophylactic approaches for this disease whose treatment management still remains a clinical challenge.

MATERIALS AND METHODS

Atopic dermatitis model

AD was induced in 8 to 12 weeks of age-matched female C57Bl/6J (WT), SphK1 KO (SphK1^{tm1Rlp}), and MC-deficient *Kit*$^{W\text{-}sh/W\text{-}sh}$ (B6.Cg-*Kit*$^{W\text{-}sh}$/HNihrJaeBsmGlliJ) mice as previously described (16), purchased from Charles River NCI (Frederick, MD) and The Jackson Laboratory (Bar Harbor, ME). After simple randomization using shuffled pieces of paper that indicated treatment, mice were assigned to either experimental group. Then, 100 μl of OVA solution (100 μg OVA (Sigma-Aldrich, St Louis, MO), LPS-free OVA (100 μg EndoGrade® OVA (Hyglos GmbH, Munich, Germany), LPS (10 or 100 μg *E. coli* LPS serotype 055:B5 (Sigma-Aldrich) (68, 69) or 0.9% saline only (shaved and tape-stripped saline control) were pipetted on a 1 cm x 1 cm square gauze pad (patch) placed on the shaved and tape-striped upper-back skin area. Next, this area was occluded with a Tegaderm Transparent Dressing (3M HealthCare, St Paul, MN) using bandages. Untreated tape-stripped, shaved, and shaved and tape-stripped skin control groups were also analyzed. Patch was removed after seven days and skin samples collected from euthanized mice. For patch 3-IgE determinations, the full AD protocol was conducted exactly as previously described (16). Briefly, each patch was secured for one week followed by two weeks of rest before next exposure week. Patch 1 and patch 3 sera were prepared from blood collected by cardiac puncture immediately after euthanasia and stored at −80°C until use. For some experiments, mice received i.p. injections of PF-543 (20 mg/kg every other day (51) (or saline vehicle) or topical application of FTY-720 (12 μg/patch area daily ((70) or methanol vehicle) at the time of saline or OVA exposure. Animal experiments and all experimental protocols were approved by the University of South Carolina Institutional Animal Care and Use Committee. Animal experiments and all methods were performed in accordance with the relevant guidelines and regulations.

Histology and Microscopy

Skin tissues collected from euthanized mice were fixed in 4% fresh paraformaldehyde, embedded in paraffin, sectioned (4 μm thickness) and mounted on microscope slides. One group of slides was stained with Hematoxylin and Eosin (H&E) for skin morphometric analysis. To visualize MC, a second group of slides was placed in 0.1% methylene blue (MB) for five seconds, rinsed with water, dehydrated in 100% ethanol and mounted under coverslips with cytoseal 60 (71). Sections were imaged with a Nikon E-600 microscope (Nikon Inc., Melville, NY) equipped with a Micropublisher digital camera model 5.0 and images collected as TIFF files with the Micropublisher software at low (10x) and high (40x) magnification. Images were analyzed as 24-bit color images or 8-bit monochrome images, using the QImaging software version 2.0.13 (QImaging Corp., Surrey, BC, Canada). Morphometric and fractal parameters of nuclei (infiltration, 25–30 ROIs/image, a minimum of twelve 40x-images/skin section; 4 skin sections/2 mice/treatment group) and MC (percent degranulation, fifty 40x- total images/310–485 total MC; 4 skin sections/2 mice/treatment group) were measured using the MetaMorph® 6.1 Microscopy Automation and Image Analysis software (Molecular Devices, Sunnyvale, CA) and the free HarFa imaging software (www.fch.vutbr.cz/lectures/imagesci/), as previously described (30). For these and all quantifications described below, the investigators who were making measurements were blind to slide group allocations (single blind studies).

Morphometric measurement of skin remodeling

The thickness of each skin layer (epidermis, dermis and hypodermis) was measured in saline- and OVA-treated specimens using an ocular micrometer (Klarmann Rulings, Inc., Litchfield, NH). From each slide, uniform regions of the epidermis, dermis and hypodermis were selected and the average thickness was measured (n= 3–5 measurements/3–5 animals/treatment group/skin layer (i.e, epidermis, dermis, hypodermis).

Computer-assisted quantification of hypodermal cellular infiltration

An imaging method developed by our laboratory (30) was adapted to quantify cellular infiltration. A minimum of twelve high-magnification H&E images per animal was used to determine cellular infiltration in the hypodermis. To this end, nuclei were isolated by means of color thresholding using the set color threshold subroutine of the MetaMorph software (orange color overlay) and quantified by applying a fixed circular region of interest (ROI, diameter=75μm) of constant area that was moved sequentially to survey the entire hypodermis of each section (n=25–30 ROIs/section, 2 sections/slide, 2 slides/animal, 2 animals/treatment). The morphometric parameters of the nuclei (area, perimeter and integrated optical density determined using the Integrated Morphometry Analysis subroutine of MetaMorph) were used to refine nuclei measurements and eliminate any background noise.

Validation of cellular infiltration quantification by independent fractal dimension analysis

As described above, fixed circular ROIs were isolated and collected as TIFF file images throughout the hypodermis of H&E images in each section. The hue, saturation and intensity values were adjusted to isolate the nuclei in orange as a thresholded region. The images of

individual nuclei (green) were converted to a 8-bit gray scale image for fractal dimension measurements, as we previously described (30). An area featuring cellular infiltration is an object composed of nuclei, which are fundamentally similar (self-similar). Because of its complexity, infiltration can be described quantitatively by fractal geometry, with values falling between two-integer topological dimensions. These numbers define the fractal dimension (D) of an “object”, here, the distribution of nuclei within a hypodermal ROI. In two-dimensional images, D values are fractional and lie between the Euclidean integers of 1 and 2.

In situ determination of mast cell degranulation

We previously demonstrated (30) that MC cytoplasm can be described quantitatively by fractal geometry, with the fractal dimension (D) value uniquely characterizing intact MCs being 1.378 ± 0.062 and the D value of degranulated MCs, 1.484 ± 0.048 (30). These values were used as a baseline for non-subjective quantification of MC activation in variously treated skin samples (n=2–5 animals/treatment).

Quantitative Real-Time qPCR

Skin samples were collected, snap-frozen and stored at −80°C until RNA extraction. Total RNA from variously treated skin samples (n=4–10 animals) was isolated and purified with the miRNeasy kit (Qiagen, Valencia, CA). The iScript cDNA synthesis kit (Bio-Rad, Hercules, CA) was used to reverse transcribe cDNA. QPCR was performed on a CFX Connect (Bio-Rad) with SensiFAST™ SYBR No-ROX Kit (Bioline, Taunton, MA). The following primers were used for real-time qPCR amplification: GAPDH forward primer CAGAAGGGGCGGAGATGAT and reverse primer AGGCCGGTGCTGCTGAGTATGTC, FcεRIα forward primer ATTGTGAGTGCCACCGTTCA and reverse primer GCAGCCAATCTTGCGTTACA, CCL2 forward primer CACTCACCTGCTGCTACTCA and reverse primer GCTTGGTGACAAAAACTACAGC, CCL3 forward primer GCCATATGGAGCTGACACCC and reverse primer TAGTCAGGAAAATGACACCTGGC, Sphk1 forward primer CGTGGACCTCGAGAGTGAGAA and reverse primer AGGCTTGCTAGGCGAAAGAAG, Sgpl1 forward primer GGTGTATGAGCTTATCTTCCAGC and reverse primer CTGTTGTTCGATCTTACGTCCA, Sgpp1 forward primer TACGGGCTGATTCTCATTCCC and reverse primer GGTCCACCAATGGGTAGAAGA, Sgpp2 forward primer CACCCACTGGAATATCGACCC and reverse primer AAGTCTCACAACGGGAGGAAA and CCL5 forward primer TGCCCTCACCATCATCCTCACT and reverse primer GGCGGTTCCTTCGAGTGACA. The real-time qPCR conditions were as follows: initial step at 95°C for 5 min and cycles (n=40) consisted of 10 s at 95°C, followed by 1 min annealing at 55°C and extension at 72°C. All reactions were performed in duplicate. Data were analyzed with CFX Manager™ Software, normalized to saline-treated samples and directly proportional to the amount of target gene mRNA relative to the amount of reference gene, GAPDH mRNA levels. Primers were purchased from Thermo Fisher Scientific, Inc. (Waltham, MA).

Multiplex Assays

Chemokines were measured in mouse serum or skin protein extracts (n=10–12 mice/treatment/sample type) with a Bio-Plex Array Reader (LUMINEX 100; Bio-Rad Laboratories, Hercules, CA) using Milliplex panels (EMD Millipore, Billerica, MA): CCL2/monocyte chemoattractant protein 1, CCL3/macrophage inflammatory protein 1α and CCL5/RANTES. Protein extracts were obtained from skin specimens harvested after one week of treatment, weighed, and frozen in liquid nitrogen. Each sample was homogenized with a mortar and pestle and digested for 2 h at 4°C in Reporter lysis buffer (Promega, Madison, WI) supplemented with complete mini-protease inhibitor tablets (Roche Diagnostics, Indianapolis, IN). Supernatants were stored at −80°C until use.

Total Serum IgE ELISA

Mouse total serum IgE was measured by ELISA (R&D Systems, Minneapolis, MN). N=6 animals/experimental groups for one exposure and n=9 animals/experimental groups for three exposures.

Lipidomics

Lipids were extracted from snap-frozen skin tissues and from saline, OVA and LPS-free OVA stock solutions used on patches and S1P was measured by using liquid chromatography-electrospray ionization-tandem mass spectrometry (4000 QTRAP; AB Sciex, Foster City, CA), as previously described (40). Quantification of S1P was normalized to weight of skin sample or volume. No detectable levels of S1P were found in any of the solutions applied on patches. N=3–4 samples per experimental group.

Statistics

Data are expressed as means + SEM (unless otherwise stated) and were analyzed by using the unpaired 2-tailed Student *t* test, with Welch's correction for samples of unequal variance (Prism 6; GraphPad Software, La Jolla, CA). Significance for all statistical tests is shown in figures. All experiments were repeated at least 3 times in triplicates with consistent results. Each *in vivo* experimental group consisted of 4 to 10 mice.

Supplementary Material

Refer to Web version on PubMed Central for supplementary material.

ACKNOWLEDGMENTS

We are grateful to Dr. Christine Tkaczyk, MedImmune, Infectious Diseases Department, Gaithersburg, MD, for generously sharing the mouse skin digestion protocol. We thank VCU Lipidomics/Metabolics Core for lipid determinations, the National Institutes of Health (NIH)/NCI Cancer Center Support Grant P30 CA016059 to the VCU Massey Cancer Center, and a shared resource grant (S10RR031535). This study was supported in part by the Higher Committee for Education Development in Iraq to AA, the University of South Carolina School of Medicine, and the National Institute of Allergy and Infectious Diseases/NIH R01 AI095494, the National Institute of Arthritis and Musculoskeletal and Skin Diseases/NIH R21 AR067996, and a National Institute of General Medical Sciences/NIH Bioinformatics Pilot Project P20 GM103499 to CAO.

ABBREVIATIONS

AD	atopic dermatitis
Ag	antigen
Bv	blood vessels
D	fractal dimension
EC	epicutaneous
H&E	hematoxylin and eosin
MC	mast cell
S1P	sphingosine-1-phosphate
SphK1	sphingosine kinase 1
Sgpl1	S1P lyase
Sgpp	S1P phosphatase
ROI	region of interest

REFERENCES

1. Auriemma M, Vianale G, Amerio P, Reale M. Cytokines and T cells in atopic dermatitis. Eur Cytokine Netw 2013;24(1):37–44. [PubMed: 23608610]
2. Darlenski R, Kazandjieva J, Hristakieva E, Fluhr JW. Atopic dermatitis as a systemic disease. Clin Dermatol 2014;32(3):409–413. [PubMed: 24767188]
3. Eyerich K, Novak N. Immunology of atopic eczema: overcoming the Th1/Th2 paradigm. Allergy 2013;68(8):974–982. [PubMed: 23889510]
4. Graham MT, Nadeau KC. Lessons learned from mice and man: mimicking human allergy through mouse models. Clin Immunol 2014;155(1):1–16. [PubMed: 25131136]
5. Liu FT, Goodarzi H, Chen HY. IgE, mast cells, and eosinophils in atopic dermatitis. Clin Rev Allergy Immunol 2011;41(3):298–310. [PubMed: 21249468]
6. Nakamura Y, Oscherwitz J, Cease KB, Chan SM, Muñoz-Planillo R, Hasegawa M, et al. Staphylococcus δ-toxin induces allergic skin disease by activating mast cells. Nature 2013;503(7476):397–401. [PubMed: 24172897]
7. Patrizi A, Pileri A, Bellini F, Raone B, Neri I, Ricci G. Atopic dermatitis and the atopic march: what is new? J Allergy (Cairo) 2011;2011:279425.
8. Szegedi K, Lutter R, Res PC, Bos JD, Luiten RM, Kezic S, et al. Cytokine profiles in interstitial fluid from chronic atopic dermatitis skin. J Eur Acad Dermatol Venereol 2015.
9. Elias PM. Lipid abnormalities and lipid-based repair strategies in atopic dermatitis. Biochim Biophys Acta 2014;1841(3):323–330. [PubMed: 24128970]
10. Kim JY, Jeong MS, Park MK, Lee MK, Seo SJ. Time-dependent progression from the acute to chronic phases in atopic dermatitis induced by epicutaneous allergen stimulation in NC/Nga mice. Exp Dermatol 2014;23(1):53–57. [PubMed: 24299269]
11. Mu Z, Zhao Y, Liu X, Chang C, Zhang J. Molecular biology of atopic dermatitis. Clin Rev Allergy Immunol 2014;47(2):193–218. [PubMed: 24715253]
12. Ando T, Matsumoto K, Namiranian S, Yamashita H, Glatthorn H, Kimura M, et al. Mast cells are required for full expression of allergen/SEB-induced skin inflammation. J Invest Dermatol 2013;133(12):2695–2705. [PubMed: 23752044]

13. Kendall AC, Nicolaou A. Bioactive lipid mediators in skin inflammation and immunity. Prog Lipid Res 2013;52(1):141–164. [PubMed: 23124022]
14. Zhu Y, Pan WH, Wang XR, Liu Y, Chen M, Xu XG, et al. Tryptase and protease-activated receptor-2 stimulate scratching behavior in a murine model of ovalbumin-induced atopic-like dermatitis. Int Immunopharmacol 2015;28(1):507–512. [PubMed: 26049029]
15. Wang G, Savinko T, Wolff H, Dieu-Nosjean MC, Kemeny L, Homey B, et al. Repeated epicutaneous exposures to ovalbumin progressively induce atopic dermatitis-like skin lesions in mice. Clin Exp Allergy 2007;37(1):151–161. [PubMed: 17210053]
16. Spergel JM, Mizoguchi E, Brewer JP, Martin TR, Bhan AK, Geha RS. Epicutaneous sensitization with protein antigen induces localized allergic dermatitis and hyperresponsiveness to methacholine after single exposure to aerosolized antigen in mice. J Clin Invest 1998;101(8):1614–1622. [PubMed: 9541491]
17. He R, Oyoshi MK, Jin H, Geha RS. Epicutaneous antigen exposure induces a Th17 response that drives airway inflammation after inhalation challenge. Proc Natl Acad Sci U S A 2007;104(40):15817–15822. [PubMed: 17893340]
18. Gittler JK, Shemer A, Suárez-Fariñas M, Fuentes-Duculan J, Gulewicz KJ, Wang CQ, et al. Progressive activation of T(H)2/T(H)22 cytokines and selective epidermal proteins characterizes acute and chronic atopic dermatitis. J Allergy Clin Immunol 2012;130(6):1344–1354. [PubMed: 22951056]
19. Griffith JW, Sokol CL, Luster AD. Chemokines and chemokine receptors: positioning cells for host defense and immunity. Annu Rev Immunol 2014;32:659–702. [PubMed: 24655300]
20. Oskeritzian CA, Price MM, Hait NC, Kapitonov D, Falanga YT, Morales JK, et al. Essential roles of sphingosine-1-phosphate receptor 2 in human mast cell activation, anaphylaxis, and pulmonary edema. J Exp Med 2010;207(3):465–474. [PubMed: 20194630]
21. Oskeritzian CA, Hait NC, Wedman P, Chumanevich A, Kolawole EM, Price MM, et al. The sphingosine-1-phosphate/sphingosine-1-phosphate receptor 2 axis regulates early airway T-cell infiltration in murine mast cell-dependent acute allergic responses. J Allergy Clin Immunol 2015;135(4):1008–1018.e1001. [PubMed: 25512083]
22. Oskeritzian CA. Mast cell plasticity and sphingosine-1-phosphate in immunity, inflammation and cancer. Mol Immunol 2015;63(1):104–112. [PubMed: 24766823]
23. Kalesnikoff J, Galli SJ. New developments in mast cell biology. Nat Immunol 2008;9(11):1215–1223. [PubMed: 18936782]
24. Galli SJ, Tsai M. IgE and mast cells in allergic disease. Nat Med 2012;18(5):693–704. [PubMed: 22561833]
25. Oskeritzian CA, Alvarez SE, Hait NC, Price MM, Milstien S, Spiegel S. Distinct roles of sphingosine kinases 1 and 2 in human mast-cell functions. Blood 2008;111(8):4193–4200. [PubMed: 18178871]
26. Mitra P, Oskeritzian CA, Payne SG, Beaven MA, Milstien S, Spiegel S. Role of ABCC1 in export of sphingosine-1-phosphate from mast cells. Proc Natl Acad Sci U S A 2006;103(44):16394–16399. [PubMed: 17050692]
27. Chumanevich A, Wedman P, Oskeritzian CA. Sphingosine-1-Phosphate/Sphingosine-1-Phosphate Receptor 2 Axis Can Promote Mouse and Human Primary Mast Cell Angiogenic Potential through Upregulation of Vascular Endothelial Growth Factor-A and Matrix Metalloproteinase-2. Mediators of Inflammation 2016;2016(Article ID 1503206):8.
28. Leung DY, Guttman-Yassky E. Deciphering the complexities of atopic dermatitis: shifting paradigms in treatment approaches. J Allergy Clin Immunol 2014;134(4):769–779. [PubMed: 25282559]
29. Malajian D, Guttman-Yassky E. New pathogenic and therapeutic paradigms in atopic dermatitis. Cytokine 2015;73(2):311–318. [PubMed: 25542094]
30. Wedman P, Aladhami A, Beste M, Edwards MK, Chumanevich A, Fuseler JW, et al. A New Image Analysis Method Based on Morphometric and Fractal Parameters for Rapid Evaluation of In Situ Mammalian Mast Cell Status. Microsc Microanal 2015;21(6):1573–1581. [PubMed: 26492872]
31. Ewald DA, Malajian D, Krueger JG, Workman CT, Wang T, Tian S, et al. Meta-analysis derived atopic dermatitis (MADAD) transcriptome defines a robust AD signature highlighting the

involvement of atherosclerosis and lipid metabolism pathways. BMC Med Genomics 2015;8:60. [PubMed: 26459294]

32. Suárez-Fariñas M, Ungar B, Correa da Rosa J, Ewald DA, Rozenblit M, Gonzalez J, et al. RNA sequencing atopic dermatitis transcriptome profiling provides insights into novel disease mechanisms with potential therapeutic implications. J Allergy Clin Immunol 2015;135(5):1218–1227. [PubMed: 25840722]
33. Metzger H, Alcaraz G, Hohman R, Kinet JP, Pribluda V, Quarto R. The receptor with high affinity for immunoglobulin E. Annu Rev Immunol 1986;4:419–470. [PubMed: 3011032]
34. Haas N, Hamann K, Grabbe J, Czarnetzki BM. Demonstration of the high-affinity IgE receptor (Fc epsilon RI) on Langerhans cells of oral mucosa. Exp Dermatol 1993;2(4):157–160. [PubMed: 8162333]
35. Ying S, Barata LT, Meng Q, Grant JA, Barkans J, Durham SR, et al. High-affinity immunoglobulin E receptor (Fc epsilon RI)-bearing eosinophils, mast cells, macrophages and Langerhans' cells in allergen-induced late-phase cutaneous reactions in atopic subjects. Immunology 1998;93(2):281–288. [PubMed: 9616380]
36. Damsgaard TE, Olesen AB, Sørensen FB, Thestrup-Pedersen K, Schiøtz PO. Mast cells and atopic dermatitis. Stereological quantification of mast cells in atopic dermatitis and normal human skin. Arch Dermatol Res 1997;289(5):256–260. [PubMed: 9164634]
37. Kawakami T, Ando T, Kimura M, Wilson BS, Kawakami Y. Mast cells in atopic dermatitis. Curr Opin Immunol 2009;21(6):666–678. [PubMed: 19828304]
38. Sehra S, Serezani AP, Ocaña JA, Travers JB, Kaplan MH. Mast Cells Regulate Epidermal Barrier Function and the Development of Allergic Skin Inflammation. J Invest Dermatol 2016;136(7):1429–1437. [PubMed: 27021404]
39. Rivera J, Proia RL, Olivera A. The alliance of sphingosine-1-phosphate and its receptors in immunity. Nat Rev Immunol 2008;8(10):753–763. [PubMed: 18787560]
40. Hait NC, Allegood J, Maceyka M, Strub GM, Harikumar KB, Singh SK, et al. Regulation of histone acetylation in the nucleus by sphingosine-1-phosphate. Science 2009;325(5945):1254–1257. [PubMed: 19729656]
41. Saba JD, Nara F, Bielawska A, Garrett S, Hannun YA. The BST1 gene of Saccharomyces cerevisiae is the sphingosine-1-phosphate lyase. J Biol Chem 1997;272(42):26087–26090. [PubMed: 9334171]
42. Le Stunff H, Giussani P, Maceyka M, Lépine S, Milstien S, Spiegel S. Recycling of sphingosine is regulated by the concerted actions of sphingosine-1-phosphate phosphohydrolase 1 and sphingosine kinase 2. J Biol Chem 1997;282(47):34372–34380.
43. Price MM, Oskeritzian CA, Falanga YT, Harikumar KB, Allegood JC, Alvarez SE, et al. A specific sphingosine kinase 1 inhibitor attenuates airway hyperresponsiveness and inflammation in a mast cell-dependent murine model of allergic asthma. J Allergy Clin Immunol 2013;131(2):501–511.e501. [PubMed: 22939756]
44. Nussbaum C, Bannenberg S, Keul P, Gräler MH, Gonçalves-de-Albuquerque CF, Korhonen H, et al. Sphingosine-1-phosphate receptor 3 promotes leukocyte rolling by mobilizing endothelial P-selectin. Nat Commun 2015;6:6416. [PubMed: 25832730]
45. Gonzalo JA, Qiu Y, Lora JM, Al-Garawi A, Villeval JL, Boyce JA, et al. Coordinated involvement of mast cells and T cells in allergic mucosal inflammation: critical role of the CC chemokine ligand 1:CCR8 axis. J Immunol 2007;179(3):1740–1750. [PubMed: 17641040]
46. Wu Z, Macneil AJ, Junkins R, Li B, Berman JN, Lin TJ. Mast cell FcεRI-induced early growth response 2 regulates CC chemokine ligand 1-dependent CD4+ T cell migration. J Immunol 2013;190(9):4500–4507. [PubMed: 23536637]
47. Ohsawa Y, Hirasawa N. The antagonism of histamine H1 and H4 receptors ameliorates chronic allergic dermatitis via anti-pruritic and anti-inflammatory effects in NC/Nga mice. Allergy 2012;67(8):1014–1022. [PubMed: 22686688]
48. McAlpine SM, Issekutz TB, Marshall JS. Virus stimulation of human mast cells results in the recruitment of $CD56^{+}$ T cells by a mechanism dependent on CCR5 ligands. FASEB J 2012;26(3):1280–1289. [PubMed: 22125314]

49. Sulcova J, Meyer M, Guiducci E, Feyerabend TB, Rodewald HR, Werner S. Mast cells are dispensable in a genetic mouse model of chronic dermatitis. Am J Pathol 2015;185(6):1575–1587. [PubMed: 25843682]
50. Allende ML, Sasaki T, Kawai H, Olivera A, Mi Y, van Echten-Deckert G, et al. Mice deficient in sphingosine kinase 1 are rendered lymphopenic by FTY720. J Biol Chem 2004;279(50):52487–52492. [PubMed: 15459201]
51. MacRitchie N, Volpert G, Al Washih M, Watson DG, Futerman AH, Kennedy S, Pyne S, Pyne NJ. Effect of the sphingosine kinase 1 selective inhibitor, PF-543 on arterial and cardiac remodelling in a hypoxic model of pulmonary arterial hypertension, Cell Signal 2016;28(8):946–955. [PubMed: 27063355]
52. Grimbaldeston MA, Chen CC, Piliponsky AM, Tsai M, Tam SY, Galli SJ. Mast cell-deficient W-sash c-kit mutant Kit W-sh/W-sh mice as a model for investigating mast cell biology in vivo. Am J Pathol 2005;167(3):835–848. [PubMed: 16127161]
53. Oizumi A, Nakayama H, Okino N, Iwahara C, Kina K, Matsumoto R, et al. Pseudomonas-derived ceramidase induces production of inflammatory mediators from human keratinocytes via sphingosine-1-phosphate. PLoS One 2014;9(2):e89402.
54. Japtok L, Schaper K, Bäumer W, Radeke HH, Jeong SK, Kleuser B. Sphingosine 1-phosphate modulates antigen capture by murine Langerhans cells via the S1P2 receptor subtype. PLoS One 2012;7(11):e49427.
55. Japtok L, Bäumer W, Kleuser B. Sphingosine-1-phosphate as signaling molecule in the skin: Relevance in atopic dermatitis. Allergo J Int 2014;23(2):54–59. [PubMed: 26120515]
56. Dillahunt SE, Sargent JL, Suzuki R, Proia RL, Gilfillan A, Rivera J, et al. Usage of sphingosine kinase isoforms in mast cells is species and/or cell type determined. J Immunol 2013;190(5):2058–2067. [PubMed: 23359503]
57. Yoon J, Leyva-Castillo JM, Wang G, Galand C, Oyoshi MK, Kumar L, et al. IL-23 induced in keratinocytes by endogenous TLR4 ligands polarizes dendritic cells to drive IL-22 responses to skin immunization. J Exp Med 2016;213(10):2147–2166. [PubMed: 27551155]
58. Watanabe J, Miyazaki Y, Zimmerman GA, Albertine KH, McIntyre TM. Endotoxin contamination of ovalbumin suppresses murine immunologic responses and development of airway hyper-reactivity. J Biol Chem 2003;278(43):42361–42368. [PubMed: 12909619]
59. Eisenbarth SC, Piggott DA, Huleatt JW, Visintin I, Herrick CA, Bottomly K. Lipopolysaccharide-enhanced, toll-like receptor 4-dependent T helper cell type 2 responses to inhaled antigen. J Exp Med 2002;196(12):1645–1651. [PubMed: 12486107]
60. Dong L, Li H, Wang S, Li Y. Different doses of lipopolysaccharides regulate the lung inflammation of asthmatic mice via TLR4 pathway in alveolar macrophages. J Asthma 2009;46(3):229–233. [PubMed: 19373628]
61. Nakatsuji T, Chen TH, Narala S, Chun KA, Two AM, Yun T, et al. Antimicrobials from human skin commensal bacteria protect against Staphylococcus aureus and are deficient in atopic dermatitis. Sci Transl Med 2017;9(378) in press.
62. Wang Z, Mascarenhas N, Eckmann L, Miyamoto Y, Sun X, Kawakami T, Di Nardo A. Skin microbiome promotes mast cell maturation by triggering stem cell factor production in keratinocytes. J Allergy Clin Immunol 2017;139(4):1205–1216.e6. [PubMed: 27746235]
63. Reines I, Kietzmann M, Mischke R, Tschernig T, Lüth A, Kleuser B, et al. Topical application of sphingosine-1-phosphate and FTY720 attenuate allergic contact dermatitis reaction through inhibition of dendritic cell migration. J Invest Dermatol 2009;129(8):1954–1962. [PubMed: 19194476]
64. Sun WY, Dimasi DP, Pitman MR, Zhuang Y, Heddle R, Pitson SM, et al. Topical Application of Fingolimod Perturbs Cutaneous Inflammation. J Immunol 2016;196(9):3854–3864. [PubMed: 27001955]
65. Sobel K, Monnier L, Menyhart K, Bolinger M, Studer R, Nayler O, Gatfield J. FTY720 phosphate activates sphingosine-1-phosphate receptor 2 and selectively couples to Gα12/13/Rho/ROCK to induce myofibroblast contraction. Mol Pharmacol 2015;87(6):916–927. [PubMed: 25762025]

66. Rahman MM, Prünte L, Lebender LF, Patel BS, Gelissen I, Hansbro PM, et al. The phosphorylated form of FTY720 activates PP2A, represses inflammation and is devoid of S1P agonism in A549 lung epithelial cells. Sci Rep 2016;6:37297. [PubMed: 27849062]

67. Bandhuvula P, Tam YY, Oskouian B, Saba JD. The immune modulator FTY720 inhibits sphingosine-1-phosphate lyase activity. J Biol Chem 2005;280(40):33697–33700. [PubMed: 16118221]

68. Ishikawa Y, Kirikae T, Hirata M, Yoshida M, Haishima Y, Kondo S, Hisatsune K. Local skin response in mice induced by a single intradermal injection of bacterial lipopolysaccharide and lipid A. Infect Immun 1991;59(6):1954–1960. [PubMed: 2037357]

69. Crompton R, Williams H, Ansell D, Campbell L, Holden K, Cruickshank S, Hardman MJ. Oestrogen promotes healing in a bacterial LPS model of delayed cutaneous wound repair. Lab Invest 2016;96(4):439–449. [PubMed: 26855364]

70. Schaper K, Dickhaut J, Japtok L, Kietzmann M, Mischke R, Kleuser B, Bäumer W. Sphingosine-1-phosphate exhibits anti-proliferative and anti-inflammatory effects in mouse models of psoriasis. J Dermatol Sci 2013;71(1):29–36. [PubMed: 23643308]

71. Wolters PJ, Mallen-St Clair J, Lewis CC, Villalta SA, Baluk P, Erle DJ, et al. Tissue-selective mast cell reconstitution and differential lung gene expression in mast cell-deficient Kit(W-sh)/Kit(W-sh) sash mice. Clin Exp Allergy 2005;35(1):82–88. [PubMed: 15649271]

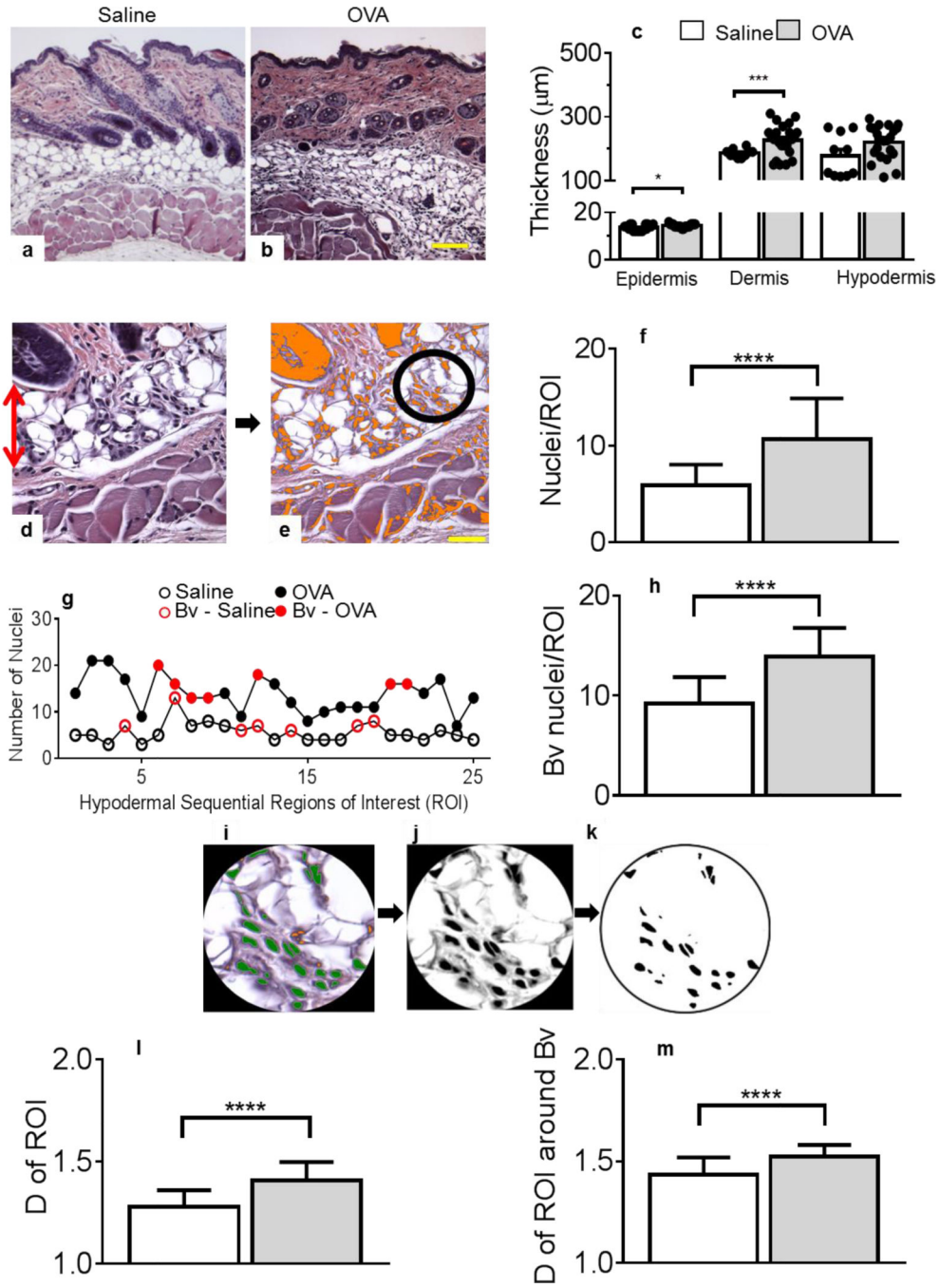

Figure 1. Skin remodeling starts after a single epicutaneous exposure to OVA.

(a-b) H&E staining of skin tissues exposed to saline (a) or OVA (b). Panels a-b are representative images. Original magnification, ×100. (c) Thickness of the epidermis, dermis and hypodermis layers, as measured in H&E-stained tissues. For epidermis thickness, n = 18 (saline, empty bars), 19 (OVA, grey bars), for dermis, n = 10 and 25 and for hypodermis, n = 10 and 25 individual measurements collected from 3–5 animals/treatment group/skin layer. (d) Example of H&E stained skin section focusing on the hypodermis (red arrow, original magnification, ×400) in which (e) nuclei are color-thresholded (orange) and a fixed circular

region of interest (ROI, black circle) defined. (f) Nuclei numbers per ROI of multiple saline treated mice, compared to OVA-treated mice. (g) Representative nuclei enumeration performed in each ROI (n = 25 ROI) throughout the hypodermis of one saline-treated mouse (empty circles) and of another exposed to OVA (filled circles). Red symbols refer to blood vessel (Bv)-containing ROI. (h) Infiltration analysis focusing around Bv. (i) Nuclei within ROI were color-thresholded as in (e) and enumerated (green). (j) Colored nuclei images were gray-scaled and (k) a binary image was software-created to calculate the fractal dimension (D) of each ROI. Panels i-k are representative images of an isolated ROI. (l) D of ROI in skin specimens treated with saline or OVA. (m) Similar determinations of D were performed focusing around Bv. For all ROI determinations, 25–30 ROIs/image, a minimum of twelve 40x-images/skin section; 4 skin sections/2 mice/treatment group were analyzed (f, h, l, m). Statistical differences were determined with unpaired 2-tailed Student's t test with Welch's correction. Bar = 50 μm. *p = 0.0142, *** p = 0.0004, **** P≤0.0001.

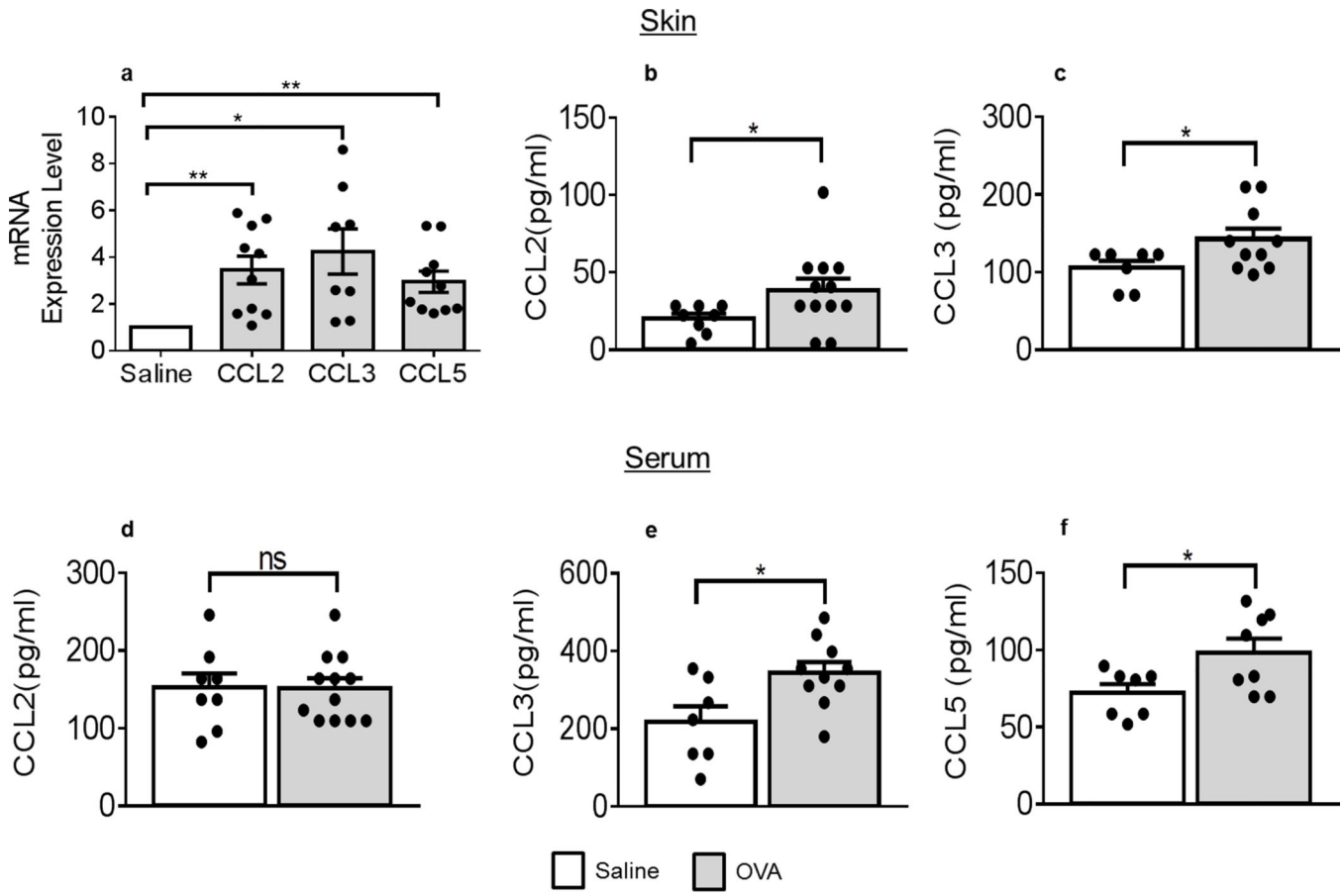

Figure 2. Chemokines are up-regulated after a single exposure to OVA.

(a) CCL2, CCL3 and CCL5 mRNA levels in OVA-treated skin samples (grey bars), normalized to those in saline-treated skins (empty bars) and quantified against GAPDH mRNA levels, n = 6 saline animals, 4–5 OVA animals with duplicate determinations. (b) CCL2 (* $p = 0.0383$) and (c) CCL3 protein levels in skin extracts (* $p = 0.0356$) (b, c) or serum (d, e: * $p = 0.0255$) and (f) serum CCL5 protein levels (* $p = 0.0307$) all collected from mice treated with saline or OVA. Protein determinations, n = 4 (saline) and 6 (OVA) with duplicate determinations. Statistical differences were determined with unpaired 2-tailed Student's t test with Welch's correction (a-f). *p ≤0.05, **p ≤0.01, except otherwise indicated; ns, not significant.

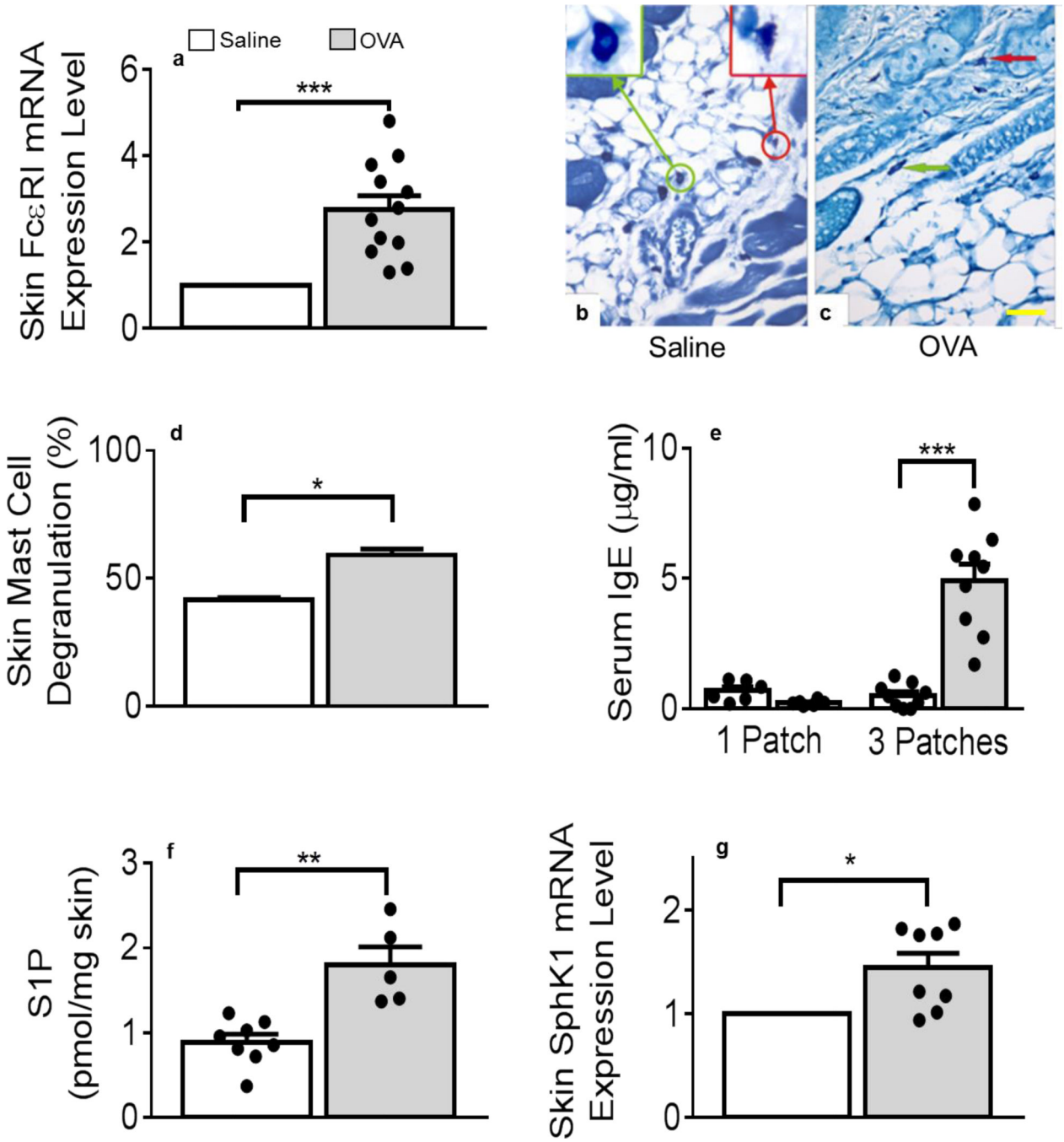

Figure 3. Mast cells degranulation and S1P levels increase in OVA-treated skin tissues.

(a) Alpha chain for the high-affinity receptor for IgE mRNA levels in OVA-treated samples (grey bars), normalized to saline (empty bars) treated samples and GAPDH, n = 4 saline animals, 6 OVA animals with duplicate determinations (*** $p = 0.0002$). (b, c) Methylene blue-stained skin sections after saline (b) or OVA (c) treatment. Arrows and inserts show examples of intact (green) or degranulated (red) mast cells (MC). Panels b-c are representative images. Bar = 50 μm. (d) Percent MC degranulation determinations in saline- and OVA-treated samples (* $p = 0.0352$, fifty 40x- total images/310–485 total MC;

4 skin sections/2 mice/treatment group). (e) Determinations of total serum IgE after one saline or OVA treatment (1 Patch), n = 6 animals/treatment group, averages of duplicate determinations and after three saline or OVA treatments (3 Patches), n = 9 animals/treatment group, averages of duplicate determinations (*** $p = 0.0001$). (f) Sphingosine-1-phosphate (S1P) content of mouse skins after saline or OVA treatment, n = 8 saline and 5 OVA samples. ** $p = 0.0088$ (g) Sphingosine kinase (SphK)1 mRNA levels in OVA-treated samples (n = 4), normalized to saline (n = 3) with duplicate measurements (* $p = 0.0152$). Statistical differences were determined with unpaired 2-tailed Student's t test with Welch's correction.

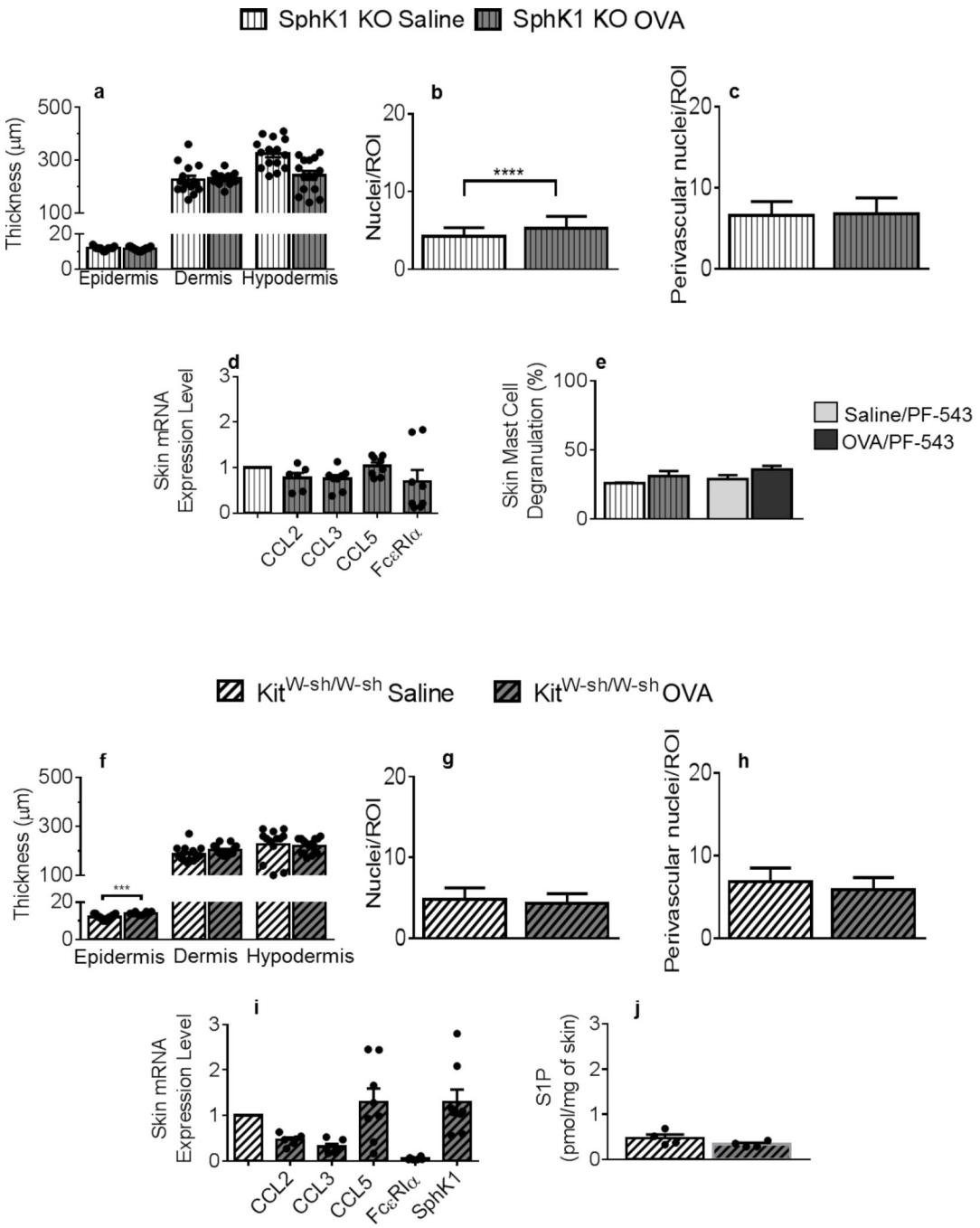

Figure 4. Skin remodeling and chemokine expression are mitigated in mice deficient for SphK1 or mast cells: S1P-mediated skin mast cell degranulation and mast cell-dependent local S1P production.

Thickness of the epidermis, dermis and hypodermis layers in SphK1 KO mice (vertical line patterns) measured in H&E-stained skin tissues. For epidermis thickness, n = 15 (saline, white bars), 15 (OVA, grey bars), for dermis, n = 15 and 13 and for hypodermis, n = 15 and 15 individual measurements collected from 3 animals/treatment group/skin layer. (b) Nuclei numbers per ROI within the hypodermis of saline-treated, compared to OVA-treated SphK1 KO mice. (c) Nuclei numbers per perivascular ROIs after saline or

OVA treatment (d) CCL2, CCL3, CCL5 and FcεRIα mRNA expression in OVA-treated (n = 3–4) compared to saline-treated (n = 4) SphK1 KO skins, normalized to GAPDH, with duplicate determinations. (e) Percent mast cell degranulation measured in MB-stained saline- or OVA-treated SphK1-KO or PF-543-treated mouse skin samples. (f) Thickness of the epidermis, dermis and hypodermis layers of Kit$^{W\text{-}sh/W\text{-}sh}$ mice (side-patterned bars), measured in H&E-stained tissues (n = 13–15 saline (white), 10–15 OVA (grey) individual measurements collected from 3 animals/treatment group/skin layer. (g) Nuclei numbers per ROI within the hypodermis of saline-treated compared to OVA-treated Kit$^{W\text{-}sh/W\text{-}sh}$ mice. (h) Nuclei numbers around perivascular ROIs. (i) CCL2, CCL3, CCL5, FcεRIα and SphK1 mRNA expression from OVA-treated normalized to saline-treated Kit$^{W\text{-}sh/W\text{-}sh}$ mouse skin samples, and to GAPDH, with duplicate determinations. (j) S1P content of Kit$^{W\text{-}sh/W\text{-}sh}$ mouse skins after saline or OVA treatment (n = 4 mice/experimental group). All measurements were conducted as described in Figures 1–3. Statistical differences were determined with unpaired 2-tailed Student's t test with Welch's correction (a-j). **** $p <$ 0.0001.

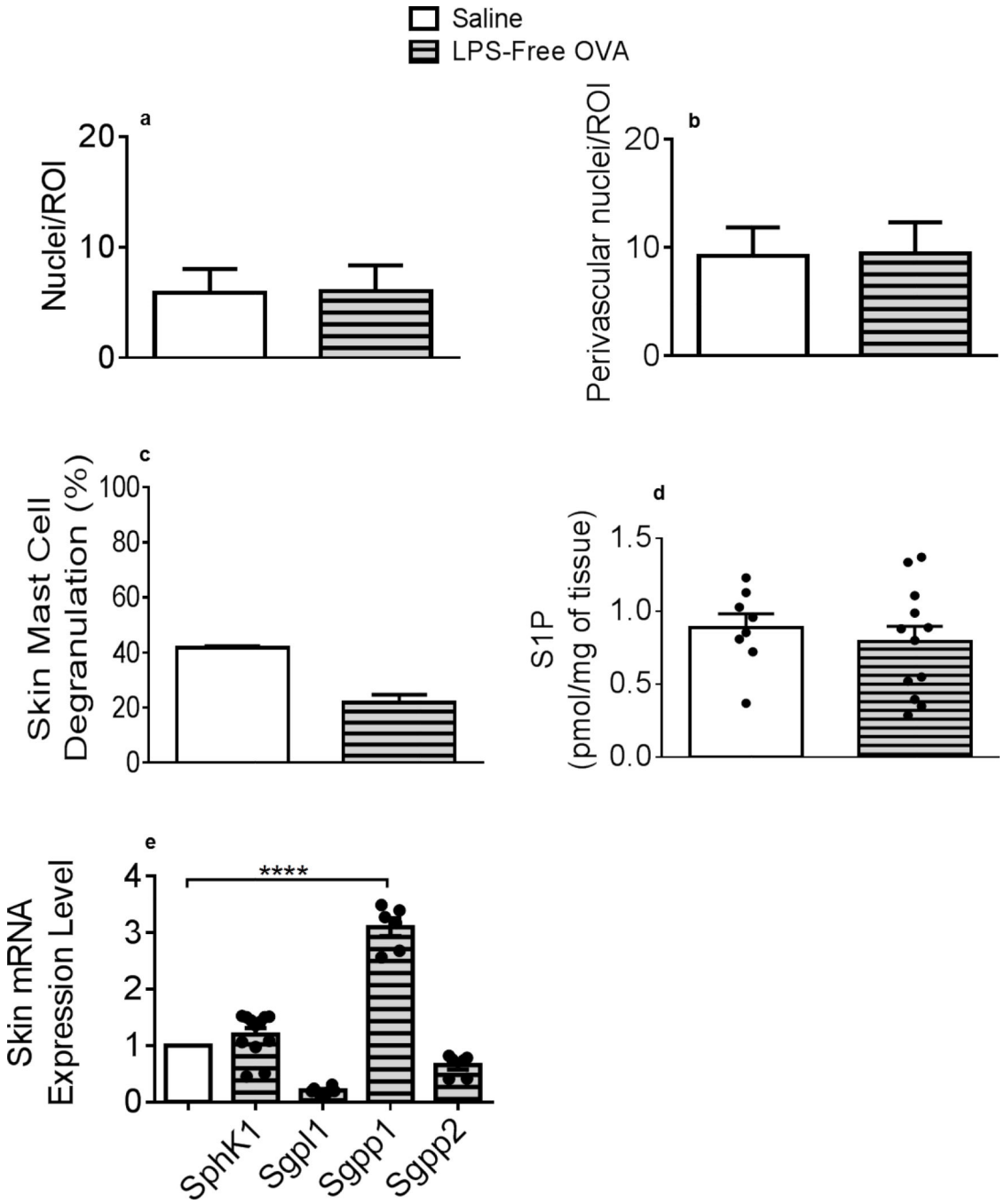

Figure 5. Cellular infiltration, mast cell degranulation and S1P increase are abated in mouse back skins exposed to LPS-free OVA.

(a) Nuclei numbers per ROI within the hypodermis of saline (empty bars)-treated compared to LPS-free OVA (horizontal-patterned grey bars)-treated mice. (b) Nuclei numbers per perivascular ROIs after saline and LPS-free OVA treatments. (a, b) 20 ROI/animal, 3 mice/ treatment. (c) Skin mast cell degranulation (%) measured in MB-stained saline- or LPS-free OVA-treated mouse skin samples. (d) S1P content of mouse skins after saline or OVA treatment. (c, d) n = 8 (saline), n = 12 (LPS-free OVA). (e) Skin SphK1, Sgpl1, Sgpp1 and Sgpp2 mRNA expression from LPS-free OVA-treated (n = 6) normalized to saline-treated

(n = 6) mouse skin samples, and to GAPDH, with duplicate determinations. Statistical differences were determined with unpaired 2-tailed Student's t test with Welch's correction (a-e). All measurements were conducted as described in Figures 1–3. **** $p < 0.0001$.